VOLUME 72, NUMBER 19 JOC Articles SEPTEMBER 14, 2007

DFT and NMR Studies of $^{2}J_{COH}$, $^{3}J_{HCOH}$, and $^{3}J_{CCOH}$ Spin-Couplings in Saccharides: C−O Torsional Bias and H-Bonding in Aqueous Solution

Hongqiu Zhao,[†] Qingfeng Pan,[†] Wenhui Zhang,[†] Ian Carmichael,[‡] and Anthony S. Serianni*,[†]

Department of Chemistry and Biochemistry and the Radiation Laboratory, University of Notre Dame, Notre Dame, Indiana 46556-5670

serianni.1@nd.edu

Received September 27, 2006

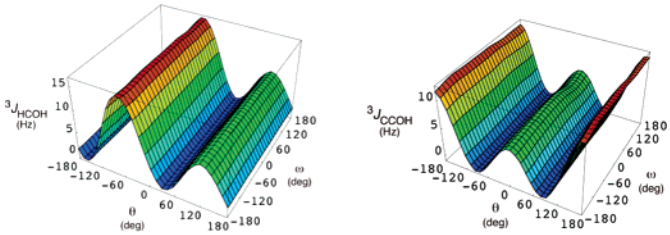

Dependence of $^{3}J_{H2,O2H}$ and $^{3}J_{C1,O2H}$ on the C2-O2 (θ) and C1-O1 (ω) torsion angles in structural mimics of β-Glc.

Density functional theory (DFT) has been used to investigate the structural dependencies of NMR spin-coupling constants (*J*-couplings) involving the exchangeable hydroxyl protons of saccharides. $^{3}J_{HCOH}$, $^{3}J_{CCOH}$, and $^{2}J_{COH}$ values were calculated at different positions in model aldopyranosyl rings as a function of one or more torsion angles, and results support the use of a generalized Karplus equation to treat $^{3}J_{HCOH}$ involving the *non-anomeric* OH groups. The presence of O5 appended to the H1−C1−O1−H coupling pathway introduces asymmetry in $^{3}J_{H1,O1H}$ Karplus curves due to internal electronegative substituent effects on the *gauche* couplings, thus requiring separate equations to treat this coupling. $^{3}J_{CCOH}$ values depend not only on the C−C−O−H torsion angle but also on the orientation of terminal substituents on the coupled carbon, similar to $^{3}J_{COCC}$ studied previously (Bose et al., *J. Am. Chem. Soc.* **1998**, *120*, 11158−11173). "In-plane" oxygen increased $^{3}J_{CCOH}$ by ∼3−4 Hz, whereas "in-plane" carbon gave more modest enhancements (∼1 Hz). Three Karplus equations were derived for non-anomeric $^{3}J_{CCOH}$ based on the nature and orientation of substituents on the coupled carbon. Like $^{3}J_{H1,O1H}$, $^{3}J_{C2,O1H}$ is also subject to internal electronegative substituent effects on the *gauche* couplings, thus necessitating separate equations to treat this coupling. $^{2}J_{COH}$ values were found not to be useful probes of C−O torsions as a result of their nonsystematic dependence on these torsions. Experimental measurements of $^{3}J_{HCOH}$ and $^{3}J_{CCOH}$ in doubly ^{13}C-labeled methyl *β*-lactoside **20** and its constituent ^{13}C-labeled methyl aldopyranosides in H_2O/acetone-d_6 at −20 °C showed that some C−O torsion angles are influenced by molecular context and do not experience complete rotational averaging in solution. A strong bias in the H3−C3−O3−H torsion angle in the Glc residue of **20** favoring a *gauche* conformation suggests the presence of inter-residue H-bonding between $O3H^{Glc}$ and $O5^{Gal}$. Quantitative analysis of $^{3}J_{HCOH}$ and $^{3}J_{CCOH}$ values in **20** indicates that ∼85% of the forms in solution have geometries consistent with H-bonding. These results suggest that H-bonding between adjacent and/or remote residues may play a role in dictating preferred glycosidic bond conformation in simple and complex oligosaccharides in aqueous solution.

Introduction

Karplus[1] first reported that vicinal $^{3}J_{HCCH}$ NMR spin−spin coupling constants (*J*-couplings) could be approximately fit to a $\cos^2\phi$ function (eq 1), where ϕ represents the H−C−C−H torsion angle, thus providing a theoretical basis for earlier

[†] Department of Chemistry and Biochemistry.
[‡] Radiation Laboratory.

(1) Karplus, M. *J. Chem. Phys.* **1959**, *30*, 11−15.
(2) Lemieux, R. U.; Kullnig, R. K.; Bernstein, H. J.; Schneider, W. G. *J. Am. Chem. Soc.* **1957**, *79*, 1005−1006.

10.1021/jo0619884 CCC: $37.00
Published on Web 02/23/2007

empirical observations made by Lemieux and co-workers.[2]

$$^3J_{HH} = A\cos^2\phi + B\cos\phi + C \quad (1)$$

Since then, additional Karplus relationships have been reported for other homonuclear *J*-couplings such as $^3J_{HCOH}$[3−5] and $^3J_{HCNH}$[6] and for heteronuclear *J*-couplings such as $^3J_{CCCH}$,[7] $^3J_{COCH}$,[8] and $^3J_{CCNH}$.[9] $^3J_{HCOH}$ and $^3J_{CCOH}$ values are potentially useful parameters to investigate intra- and/or intermolecular hydrogen bonding in OH-containing structures in solution, but relatively few studies, especially of $^3J_{CCOH,}$ have been reported on their parametrization and application in carbohydrates.[10]

Mono- and oligosaccharides contain several conformational domains, including ring, linkage, exocyclic hydroxymethyl, and/or exocyclic C−O bond conformations. Redundant trans-glycoside *J*-couplings ($^2J_{COC}$, $^3J_{COCH}$, and $^3J_{COCC}$) have been investigated as probes of C−O bond conformation in glycosidic linkages.[11a−c] Studies of redundant J_{HH}, J_{CH}, and J_{CC} within the exocyclic hydroxymethyl (CH_2OH) group of saccharides have revealed a dual dependence of some *J*-couplings on C−C and C−O torsion angles, leading to their application to evaluate correlated conformations.[12] For example, $^2J_{C5,H6R/S}$, $^2J_{C6,H5}$, and $^2J_{H6R,H6S}$ serve as probes of C6−O6 bond conformation in aldohexopyranosyl rings even though they do not involve the exchangeable O6H proton as a coupled nucleus.

$^2J_{COH}$, $^3J_{HCOH}$, and $^3J_{CCOH}$ involving exchangeable hydroxyl protons are available to confirm and/or refine conclusions based on the above-noted indirect probes of C−O bond conformation. Karplus equations for $^3J_{HCOH}$ based on experimental and computational approaches[3−5] have been reported using small, non-carbohydrate molecules such as methanol as model structures. $^3J_{CCOH}$ values have been used qualitatively to determine C−O torsion angles,[10c,13] although little is known about their dependence on saccharide structure.

In this investigation, density functional theory (DFT) has been applied to study the effects of molecular structure on $^2J_{COH}$, $^3J_{HCOH}$, and $^3J_{CCOH}$ in model aldopyranosyl rings, leading to new Karplus equations for $^3J_{HCOH}$ and $^3J_{CCOH}$. Ring configuration and pathway location were found to exert minimal effects on non-anomeric $^3J_{HCOH}$, but different equations were required to treat $^3J_{H1,O1H}$. $^3J_{CCOH}$ values show a primary dependence on the C−C−O−H torsion angle as expected but also show significant secondary dependencies on the orientation of terminal electronegative substituents attached to the coupled carbon, reminiscent of $^3J_{CCOC}$,[13,14] and on electronegative substituents appended to the internal carbon (C2−C1−O1−H torsion only). These new equations were applied to investigate intramolecular H-bonding in a doubly ^{13}C-labeled β-(1→4)-linked disaccharide in H_2O−acetone and DMSO solutions. We show that persistent inter-residue H-bonding exists in both solvents, a result having important implications for the identification of structural factors influencing the conformation and dynamics of glycosidic linkages in solution.

Computational Methods

Model compounds were chosen to mimic methyl α- and β-D-aldohexopyranosides (**1**−**4**, **9**−**14**) and α- and β-D-aldohexopyranoses (**5**−**8**) (Scheme 1). Torsion angles, ω and θ, are defined as O5−C1−O1−CH_3 (or O5−C1−O1−H) and C1−C2−O2−H, respectively (Scheme 1). Density functional theory (DFT) calculations using the B3LYP functional[15] and 6-31G* basis set[16] were conducted within *Gaussian*98[17] for geometric optimization of molecular structures.[11b,18] *J*-Couplings were calculated by DFT using a modified version of *Gaussian*94[19] and an extended basis set ([5s2p1d|3s1p])[20] designed to recover only the Fermi contact (FC) contribution to the coupling.

Three series of calculations were conducted using the above protocol. In the first, $^3J_{H2,O2H}$ and $^3J_{C1,O2H}$ were calculated in the methyl glycosides **1**−**4**. Torsion angles ω and θ were varied from 0° to 360° in 30° increments by holding both angles at fixed values, giving 144 structures for each compound. All remaining molecular parameters were geometrically optimized. $^3J_{H2,O2H}$ and $^3J_{C1,O2H}$ were calculated in each structure, yielding a hypersurface from which the relative sensitivities of the *J*-couplings to ω and θ were determined.

The second series of calculations was conducted on **5**−**8**, which contain a free anomeric hydroxyl group, to determine the effect of hydroxyl character (1°, 2°, or anomeric) on $^3J_{H1,O1H}$ and $^3J_{C2,O1H}$. Initial θ values of ∼180° were chosen to eliminate intramolecular H-bonding between O1 and O2. During geometric optimization, θ remained at ∼180° in all structures. The torsion angle ω was varied from 0° to 360° in 30° increments, and all remaining molecular parameters were optimized.

The third series of calculations was conducted on **9**−**12** to study the effect of O3 on $^3J_{H2,O2H}$, $^3J_{C1,O2H}$, and/or $^3J_{C3,O2H}$. Initial C2−C1−O1−CH_3 and C2−C3−O3−H torsion angles were set at 180° and optimized (these torsions remained at ∼180° in the optimized geometries). Values of θ were fixed at 60°, −60°, and 180°, and all remaining molecular parameters were optimized.

J-Couplings were also calculated using *Gaussian*03[21] in which both the Fermi and non-Fermi contact contributions were evaluated. DFT-optimized structures of **2** obtained from *Gaussian*98 were used, and $^3J_{H2,O2H}$, $^3J_{C1,O2H}$, and $^3J_{C3,O2H}$ values were calculated. *Gaussian*03 was also used to calculate $^3J_{H6R,O6H}$, $^3J_{H6S,O6H}$, and $^3J_{C5,O6H}$ values in **13**. In this case, the C5−C6−O6−H and O5−

(3) Fraser, R. R.; Kaufman, M.; Morand, P.; Govil, G. *Can. J. Chem.* **1969**, *47*, 403−409.
(4) Fukui, H.; Baba. T.; Inomata, H.; Miura, K.; Matsuda, H. *Mol. Phys.* **1997**, *92*, 161−165.
(5) Alkorta, I.; Elguero, J. *Theor. Chem. Acc.* **2004**, *111*, 31−35.
(6) Vuister, G. W.; Bax, A. *J. Am. Chem. Soc.* **1993**, *115*, 7772−7777.
(7) Tvaroska, I.; Gadjos, J. *Carbohydr. Res.* **1995**, *271*, 151−162.
(8) (a) Mulloy, B.; Frenkiel, T. A.; Davies, D. B. *Carbohydr. Res.* **1988**, *184*, 39−46. (b) Tvaroska, I.; Hricovini, H.; Petrakova, E. *Carbohydr. Res.* **1989**, *189*, 359−362.
(9) Hennig, M.; Bermel, W.; Schwalbe, H.; Griesinger, C. *J. Am. Chem. Soc.* **2000**, *122*, 6268−6277.
(10) (a) Adams, B.; Lerner, L. *J. Am. Chem. Soc.* **1992**, *114*, 4827−4829. (b) Sandström, C.; Basumann, L.; Kenne, J. *J. Chem. Soc., Perkin Trans. 2* **1998**, 809−815. (c) Batta, G.; Kövér, K. E. *Carbohydr. Res.* **1999**, *320*, 267−272.
(11) (a) Bose, B.; Zhao, S.; Stenutz, R.; Cloran, F.; Bondo, P. B.; Bondo, G.; Hertz, B.; Carmichael, I.; Serianni, A. S. *J. Am. Chem. Soc.* **1998**, *120*, 11158−11173. (b) Cloran, F.; Carmichael, I.; Serianni, A. S. *J. Am. Chem. Soc.* **1999**, *121*, 9843−9851. (c) Cloran, F.; Carmichael, I.; Serianni, A. S. *J. Am. Chem. Soc.* **2000**, *122*, 396−397.
(12) Thibaudeau, C.; Stenutz, R.; Hertz, B.; Klepach, T.; Zhao, S.; Wu, Q.; Carmichael, I.; Serianni, A. S. *J. Am. Chem. Soc.* **2004**, *126*, 15668−15685.
(13) Carmichael, I.; Chipman, D. M.; Podlasek, C. A.; Serianni, A. S. *J. Am. Chem. Soc.* **1993**, *115*, 10863−10870.
(14) Podlasek, C. A.; Wu, J.; Stripe, W. A.; Bondo, P. B.; Serianni, A. S. *J. Am. Chem. Soc.* **1995**, *117*, 8635−8644.
(15) Becke, A. D. *J. Chem. Phys.* **1993**, *98*, 5648−5652.
(16) Hehre, W. J.; Ditchfield, R.; Pople, J. A. *J. Chem. Phys.* **1972**, *56*, 2257−2261.
(17) Frisch, M. J. et al. *Gaussian98*, Revision A.9; Gaussian, Inc.: Pittsburgh, PA, 1998.
(18) (a) Cloran, F.; Carmichael, I.; Serianni, A. S. *J. Phys. Chem.* **1999**, *19*, 3783−3795. (b) Cloran, F.; Zhu, Y.; Osborn, J.; Carmichael, I.; Serianni, A. S. *J. Am. Chem. Soc.* **2000**, *122*, 6435−6448. (c) Cloran, F.; Carmichael, I.; Serianni, A. S. *J. Am. Chem. Soc.* **2001**, *123*, 4781−4791.
(19) Frisch, M. J. et al. *Gaussian94*; Gaussian, Inc.: Pittsburgh, PA, 1995.
(20) Stenutz, R.; Carmichael, I;. Widmalm, G.; Serianni, A. S. *J. Org. Chem.* **2002**, *67*, 949- 958.
(21) Frisch, M. J. et al. *Gaussian03*, Revision A.1; Gaussian, Inc., Pittsburgh PA, 2003.

SCHEME 1

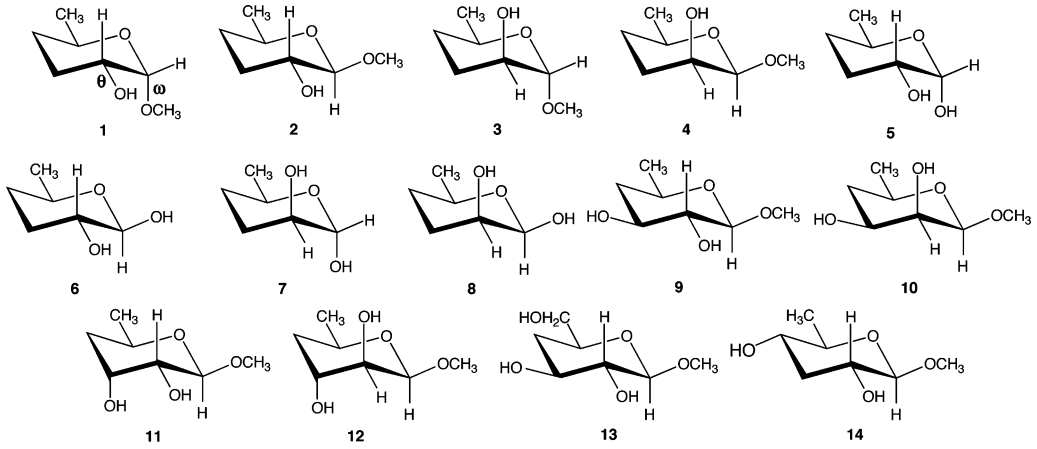

C5−C6−O6 torsion angles were fixed at 60°, −60° ,and 180°, yielding nine structures in which the three couplings were computed.

The effect of solvent water on $^3J_{HCOH}$, $^3J_{CCOH}$, and other *J*-couplings in **13** was evaluated using the self-consistent reaction field (SCRF) and the integral equation formalism (polarizable continuum) model (IEFPCM) and the above-noted [5s2p1d|3s1p] basis set as implemented in *Gaussian*03. A single optimized structure was studied containing the following exocyclic torsion angles: C2−C1−O1−CH_3, 170.4°; C1−C2−O2−H, −167.7°; C2−C3−O3−H, −165.2°; O5−C5−C6−O6, 180°; and C5−C6−O6−H, 180° (the former three torsions were relaxed and the latter two were fixed). A similar set of calculations on **13** was conducted *in vacuo*.

$^3J_{C5,O4H}$ calculations were conducted using model compound **14**. Initial C2−C1−O1−CH_3 and C1−C2−O2−H torsion angles were set at 180° and allowed to optimize (in the optimized geometries, these torsion angles remained in *anti* orientations), and the C5−C4−O4−H torsion angle was fixed at 60°, −60°, and 180°.

Experimental Section

Methyl *β*-D-glucopyranoside **15** and methyl *β*-D-galactopyranoside **16** were purchased from Sigma and used without further purification. Methyl *β*-lactoside **17**, methyl *β*-D-[4-^{13}C]glucopyranoside **18**, methyl *β*-D-[1-^{13}C]galactopyranoside **19**, and methyl *β*-[1,4′-$^{13}C_2$]lactoside **20** were synthesized as described previously.[22] Acetone-d_6 and DMSO-d_6 (99.9 atom % ^{2}H) were purchased from Cambridge Isotope Laboratories.

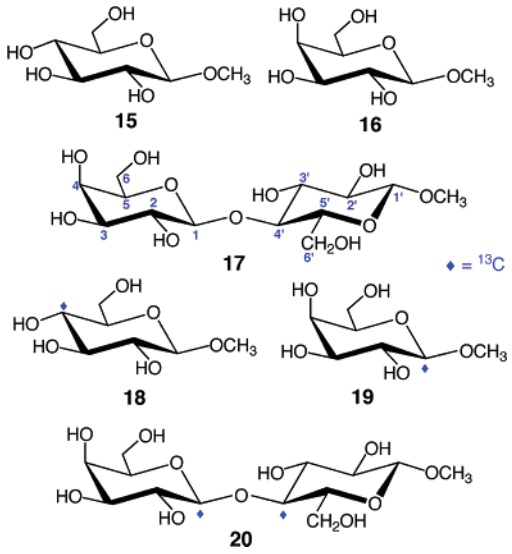

NMR samples in H_2O/acetone-d_6 solvent were prepared to minimize the presence of contaminants that could catalyze hydroxyl proton exchange.[10a] Distilled H_2O was deionized and ultrafiltered to a resistance >18 MΩ using a Millipore Milli-Q apparatus, degassed at aspirator pressure in an ultrasonic bath, and saturated with N_2 gas. NMR tubes (3 mm) were soaked for a minimum of 1 h in 50 mM sodium phosphate buffer (pH 7), rinsed with high resistance distilled water, and dried under a stream of N_2. NMR samples were prepared in a sealed glove box under an argon atmosphere using the degassed H_2O and NMR tubes described above. Solute concentration was ∼50 mM for all samples. A 1:1 (v/v) H_2O/acetone-d_6 solvent was used for the monosaccharides, and 1:1 or 2:3 (v/v) H_2O/acetone-d_6 solvents were used for the disaccharides.

NMR experiments were performed on a 600 MHz NMR spectrometer at −20 °C to reduce the exchange rate between bulk H_2O and the solute hydroxyl protons. 1D ^{1}H NMR spectra were collected with no water suppression using an 8000 Hz spectral window and a recycle time of 3 s. FIDs were zero-filled twice to give final digital resolutions of ∼0.06 Hz/pt and were Fourier transformed with (^{13}C-labeled samples) or without (unlabeled samples) weighting functions depending on the spectral resolution. Resolution enhancement weighting functions (e.g., lb = −1.0, gf = 0.8) were applied to help resolve small couplings not directly observed in unweighted spectra.

2D ^{1}H−^{1}H TOCSY spectra were obtained with a spectral window of 2400 Hz in both dimensions, H_2O presaturation, and a 65 ms mixing time. The initial matrix (2 K × 256) was zero-filled to yield a final 4 K × 2 K matrix apodized with a Gaussian function in both dimensions.

Results and Discussion

I. Theoretical Studies. A. Coupling between H2 and O2H in 1−4 and 9−12. Compounds **1**−**4** were selected as glycoside mimics to reduce complications caused by intramolecular H-bonding between adjacent hydroxyl groups. $^3J_{H2,O2H}$ values were calculated in these structures as a function of C2−O2 (*θ*) and C1−O1 (*ω*) (Scheme 1) bond rotation (Figure 1). As

(22) Synthesis of **18** and **19**: see ref 14 and refs therein. For **17**: see ref 23. For **20**: A detailed description will be reported elsewhere. Briefly, methyl *β*-D-[4-^{13}C]glucopyranoside was prepared from D-[4-^{13}C]glucose via Fischer glycosidation using Dowex 50 (H^+) ion exchange resin as a catalyst. The methyl glycoside was converted to its 2,3,6-tri-*O*-benzyl derivative via a 2,3-di-*O*-benzyl-4,6-*O*-benzyidene intermediate. The tribenzyl derivative was condensed with 2,3,4,6-tetra-*O*-acetyl-D-[1-^{13}C]galactopyranosyl trichloroacetimidate in the presence of a TMSOTf catalyst; the imidate was prepared from D-[1-^{13}C]galactose. Deprotection with NaOMe and Pt-C/H_2 afforded **20**, which was identified by its characteristic ^{13}C chemical shifts.[23]

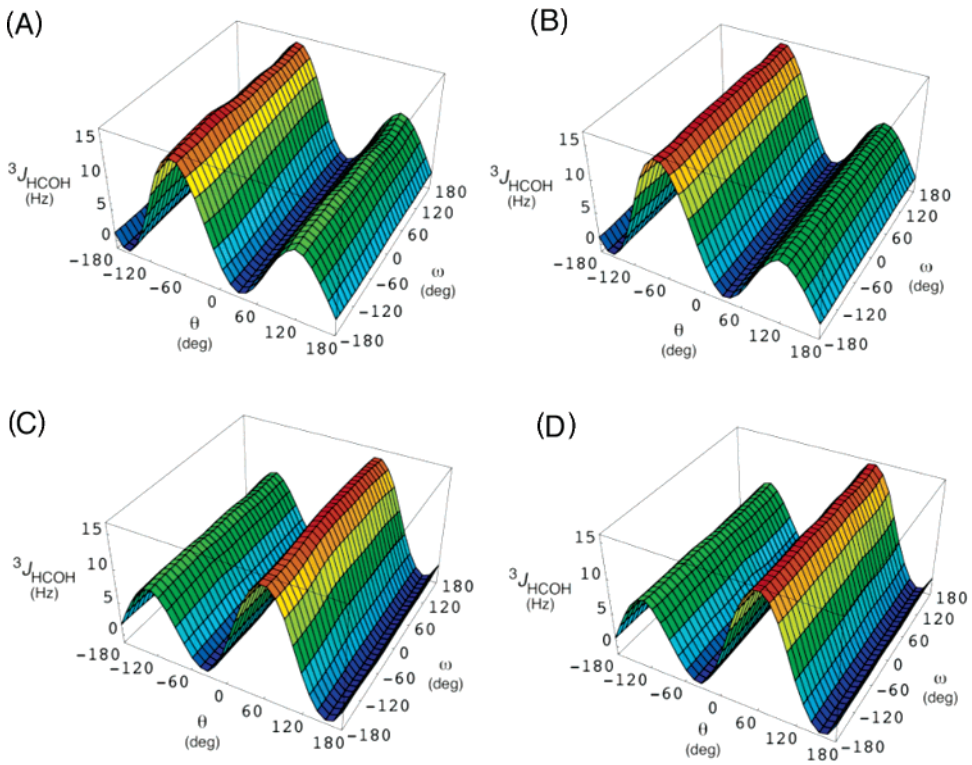

FIGURE 1. Dependence of $^3J_{H2,O2H}$ on ω and θ determined by DFT for **1** (A), **2** (B), **3** (C), and **4** (D). Note the strong dependence on θ and minimal dependence on ω.

expected, $^3J_{H2,O2H}$ exhibits a primary dependence on θ, and a small secondary dependence on ω. Plots for **1** and **2** and for **3** and **4** were nearly identical, demonstrating that $^3J_{H2,O2H}$ values are unaffected by anomeric configuration. All hypersurfaces show a global maximum of ~15 Hz at an H2−C2−O2−H torsion angle Θ of 180° and a local maximum of ~10 Hz at Θ = 0°. Portions of the hypersurfaces from Θ = 0° to180° and Θ = 0° to −180° were superimposable.

$^3J_{H2,O2H}$ values in **1**−**4** are combined and plotted in two dimensions as a function of Θ in Figure 2A (black line). The four data sets are superimposable, indicating that $^3J_{H2,O2H}$ is unaffected by C2−O2 bond orientation.

Using data in Figure 1, a least-squares fitted Karplus equation (eq 2) was obtained in which only the Fermi contact contribution to the coupling was considered (see below). The fitted curve is shown in Figure 2A. This equation is similar to eq 3 reported by Fraser et al.[3] (Figure 2A) based on theoretical calculations on CH_3OH and experimental data obtained on an H-bonded system in C^2HCl_3 solvent to constrain C−O torsions, although noticeable differences exist at the larger dihedral angles.

$$^3J_{HCOH} = 6.06 - 3.26\cos\Theta + 6.54\cos(2\Theta) \qquad R^2 = 0.99 \text{ (FC only)} \quad (2)$$

$$^3J_{HCOH} = 10.4\cos^2\Theta - 1.5\cos\Theta + 0.2 \quad (3)$$

Parametrizations for methanol based on theoretical calculations have been reported recently by Fukui et al.[4] and Alkorta and Elguero[5] (Figure 2A). These curves are also in good agreement with the present results except for couplings associated with ~180° torsion angles. Similar deviations at 180° were noted in the recent parametrization of $^3J_{COCH}$ Karplus curves based on DFT calculations.[11b]

J-Coupling calculations were conducted on **9**−**12** for a limited set of C1−O1, C2−O2, and C3−O3 torsion angles to study the effect of a C3 hydroxyl group on $^3J_{H2,O2H}$. These data, shown in Figure 2B superimposed on the parametrized curve described by eq 2, indicate that O3, whether axial or equatorial, exerts a minimal effect on $^3J_{H2,O2H}$.

B. Non-Fermi Contact Contributions to $^3J_{HCOH}$. $^3J_{H2,O2H}$ values were calculated in **2** as a function of Θ using *Gaussian*03 to determine whether non-Fermi contact (NFC) terms are important contributors to $^3J_{HCOH}$. Results obtained from *Gaussian*94 were identical to those obtained from *Gaussian*03 when only the FC contribution was recovered in the latter calculations (Figure 3). The non-Fermi contact (NFC) contribution is composed of spin-dipolar (SD), paramagnetic spin-orbital (PSO), and diamagnetic spin-orbital (DSO) terms. As shown in Figure 3, the SD term is negligible, whereas the PSO and DSO terms have opposite signs and comparable magnitudes. The sum of the PSO and DSO terms is small but non-zero, leading to a small reduction in $^3J_{H2,O2H}$ for Θ = 60°−300°, and a small increase for Θ near 0°. This result required that eq 2 be modified to account for the small NFC contribution, yielding eq 4:

$$^3J_{HCOH} = 5.76 - 2.05\cos\Theta + 6.78\cos(2\Theta) \qquad R^2 = 0.99 \text{ (FC and NFC)} \quad (4)$$

C. $^3J_{HCOH}$ Involving the C1−O1 Bond. A unique feature of the H1−C1−O1−H coupling pathway (see **Ia**) is the presence of an electronegative substituent (O5) that aligns *anti* to the coupled proton in one of the two *gauche* conformations (see **Ib** and **Ic**). This *anti* alignment (**Ib**) reduces the $^3J_{HCOH}$ in this structure, thus rendering the magnitudes of the two *gauche* couplings nonequivalent and causing the derived Karplus curve to be phase-

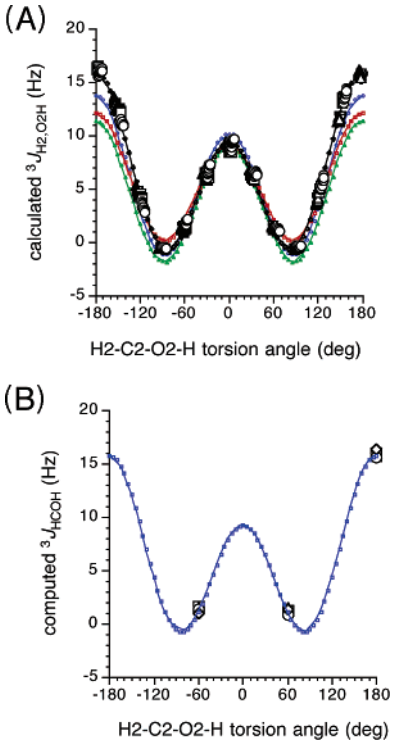

FIGURE 2. (A) Dependence of $^3J_{H2,O2H}$ on the H2−C2−O2−H torsion angle Θ in **1**−**4**; all data points are superimposed to illustrate similar *J*-couplings in each configuration. The curve fit to these data (eq 2) is indicated by the black line. Curves in red, green, and blue are those reported by Fraser et al.,[3] Alkorta and Elguero,[5] and Fukui et al.,[4] respectively. (B) Curve showing the dependence of $^3J_{H2,O2H}$ on the H2−C2−O2−H torsion angle in **1**−**4** (eq 2, blue curve) on which are superimposed computed $^3J_{H2,O2H}$ in **9**−**12** for H2−C2−O2−H torsion angles of 60°, −60°, and 180°.

shifted relative to that predicted by eq 4 (Figure 4A). The direction of the shift depends on anomeric configuration. This shifting leads to modified eqs 5 and 6 to treat $^3J_{H1,O1H}$ in α- and *β*-pyranoses, where Θ is the H1−C1−O1−H torsion angle.

$$^3J_{H1,O1H}(\alpha) = 5.52 - 2.93\cos\Theta + 6.71\cos(2\Theta) + 0.14\sin\Theta - 1.00\sin(2\Theta) \quad R^2 = 0.99 \quad (5)$$

$$^3J_{H1,OH1}(\beta) = 5.71 - 2.88\cos\Theta + 6.65\cos(2\Theta) - 0.076\sin\Theta + 1.17\sin(2\Theta) \quad R^2 = 0.99 \quad (6)$$

D. Coupling Between C1 and O2H in 1−4. $^3J_{CCOH}$ values in **1**−**4** were investigated as a potential source of C−O torsional information complementary to that obtained from $^3J_{HCOH}$. $^3J_{C1,O2H}$ values were calculated as a function of ω and θ (Figure 5). Like $^3J_{H2,O2H}$, $^3J_{C1,O2H}$ values depend mainly on θ, with ω

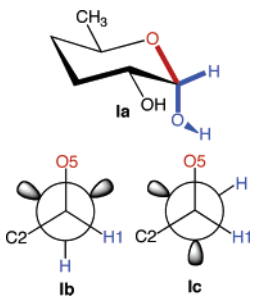

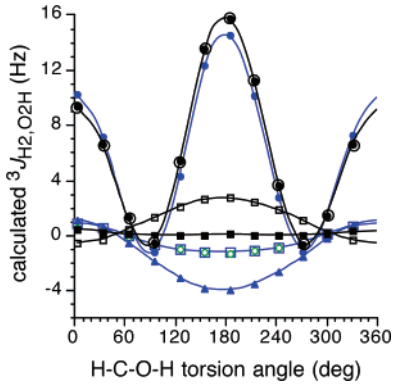

FIGURE 3. Fermi contact (FC) and non-Fermi contact (NFC) contributions to $^3J_{H2,O2H}$ in **2** computed by *Gaussian*94 (G94) and *Gaussian*03 (G03) as a function of the H2−C2−O2−H torsion angle. Black filled circles, FC (G94). Open black circles, FC (G03). Filled black squares, SD term (G03). Black open squares, PSO term (G03). Blue filled triangles, DSO term (G03). Filled blue circles, FC + NFC. Green open circles, DSO + PSO. Blue open squares, total NFC.

exerting a minor effect in all four ring configurations. All curves are symmetric about 0° and show a local maximum of ∼6 Hz at $\theta = 0°$ (Figure 6). Interestingly, the global maximum at $\theta = 180°$ depends on ring configuration, with **1**−**3** yielding values of 12−14 Hz (Figure 6A), and **4** giving a value of ∼8 Hz (Figure 6B). Separate Karplus equations were parametrized for **1**−**4** by least-squares fitting, giving eqs 7−10:

For **1**: $$^3J_{C1,O2H} = 4.02 - 2.21\cos\theta + 4.85\cos(2\theta) \quad R^2 = 0.97 \quad (7)$$

For **2**: $$^3J_{C1,O2H} = 4.02 - 2.51\cos\theta + 4.86\cos(2\theta) \quad R^2 = 0.98 \quad (8)$$

For **3**: $$^3J_{C1,O2H} = 4.20 - 3.32\cos\theta + 5.20\cos(2\theta) \quad R^2 = 0.97 \quad (9)$$

For **4**: $$^3J_{C1,O2H} = 3.28 - 0.93\cos\theta + 3.74\cos(2\theta) \quad R^2 = 0.99 \quad (10)$$

Because eqs 7−9 are very similar, they were combined to give a generalized eq 11:

For **1**−**3**: $$^3J_{C1,O2H} = 4.10 - 2.72\cos\theta + 5.01\cos(2\theta) \quad R^2 = 0.97 \quad (11)$$

The unique behavior of $^3J_{C1,O2H}$ in **4** appears to derive from the effect of terminal electronegative substituents on the coupled carbon, which is a factor known to influence other carbon-based *J*-couplings (e.g.,$^3J_{COCC}$).[11a] For **1**−**3**, an oxygen substituent is *anti* to O2 ("in-plane" substituent): O5 in **1**−**2** and O1 in **3** (Scheme 2). An in-plane orientation is absent in **4**. By analogy to $^3J_{COCC}$, terminal in-plane electronegative substituents are expected to enhance $^3J_{CCOH}$ values when the coupled atoms are approximately *anti*. $^3J_{CCOH}$ values exhibit this behavior, and the enhancement is considerably larger (3−4 Hz) than that observed for $^3J_{COCC}$ (∼0.7 Hz).[11a]

$^3J_{C1,O2H}$ values in **2** were computed using *Gaussian*03 to determine the effect of NFC terms on the computed couplings (Figure S1, Supporting Information). Unlike $^3J_{HCOH}$, the cal-

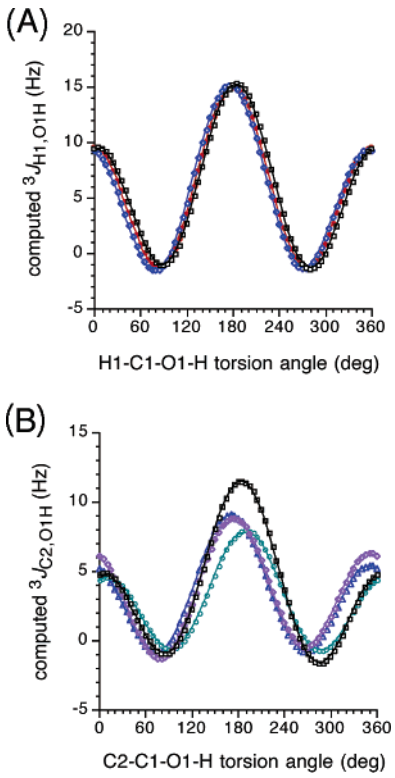

FIGURE 4. (A) Dependence of $^3J_{H1,O1H}$ on the C1−O1 bond torsion in **5**/**7** (blue triangles) and **6**/**8** (black squares). Data are superimposed on the curve derived from eq 4 (red circles). (B) Dependence of $^3J_{C2,O1H}$ on the C1−O1 torsion angle in **5** (green circles), **6** (blue triangles), **7** (black squares), and **8** (purple diamonds).

culated couplings were virtually unaffected by the inclusion of these terms. Thus, eqs 10 and 11, which were derived using only the FC term, appear suitable for the analysis of $^3J_{CCOH}$ values in saccharides.

E. C−C−O−H Coupling Pathways in 5−12. Parametrization of the $^3J_{CCOH}$ Karplus eqs 10−11 was based on the behavior of a single coupling pathway in **1**−**4**. The applicability of these equations to other C−C−O−H pathways was determined by examining (a) $^3J_{C2,O1H}$ in **5**−**8**, (b) $^3J_{C5,O4H}$ in **14**, (c) $^3J_{C1,O2H}$ in **5**−**8**, and (d) $^3J_{C1,O2H}$ in **9**−**12**. Only staggered C−C−O−H torsion angles were examined in these structures.

A terminal in-plane electronegative substituent effect was observed for $^3J_{C2,O1H}$. For example, couplings in **5**, **6**, and **8** were smaller than in **7** for C2−C1−O1−H torsions near 180° (Figure 7). However, like $^3J_{H1,OH1}$, $^3J_{C2,OH1}$ values are affected by the presence of an *internal* electronegative substituent (O5), thus necessitating separate equations to treat them (see discussion below). Couplings involving C5 ($^3J_{C5,O4H}$) were indistinguishable from those involving C1 and C2, and as expected, the in-plane O5 enhances $^3J_{C5,O4H}$ (Figure 7). The effect of methyl glycosidation on $^3J_{C1,O2H}$ is small. Finally, the presence of hydroxyl groups at C3 (structures **9**−**12**) does not affect $^3J_{C1,O2H}$ values significantly. Structures **9**−**12** also exhibit in-plane electronegative substituent effects on $^3J_{C1,O2H}$ similar to those observed in **1**−**4** (Figure 7).

The behavior of $^3J_{C2,O3H}$ and $^3J_{C3,O2H}$ in **9**−**12** is consistent with that of $^3J_{C1,O2H}$ and $^3J_{C5,O4H}$ in the same structures (Figure 8). The former couplings exhibit in-plane electronegative substituent effects (e.g., $^3J_{C3,O2H}$ is smaller in **9**, **10**, and **11** than in **12**).

Closer examination of $^3J_{C3,O2H}$ in **9**−**11** suggests the presence of a small in-plane terminal substituent effect from carbon. For C−C_x−C−O−H_x coupling pathways (subscript denotes the coupled nuclei) containing two internal trans dihedral angles (a zigzag coplanar arrangement, e.g., C4−C3−C2−O2−H in **9**), a modification of eq 10, which applies to pathways devoid of terminal carbon and oxygen in-plane substituents, is necessary, yielding eq 12:

$$^3J_{CCOH} = 3.49 - 1.41\cos\theta + 4.18\cos(2\theta) \quad R^2 = 0.99 \tag{12}$$

$$^3J_{CCOH} = 3.38 - 1.24\cos\theta + 3.98\cos(2\theta) \quad R^2 = 0.99 \tag{13}$$

An additional eq 13 was also derived, which represents an average of eqs 10 and 12. Since the in-plane terminal carbon effect is small, this averaged equation could be applied to simplify the treatment of $^3J_{CCOH}$ in saccharides (i.e., only eqs 11 and 13 are needed instead of three), with only a small loss in accuracy.

F. $^3J_{CCOH}$ Involving the C1−O1 Bond. The behavior of $^3J_{C2,O1H}$ (structure **IIa**) mimics that of $^3J_{H1,O1H}$ with respect to the effects of internal electronegative substituents. One of the *gauche* couplings (**IIb**) is influenced by the *anti*-oriented O5, whereas the other (**IIc**) is not, leading to asymmetry in the $^3J_{C2,O1H}$ Karplus curve. Superimposed on this effect is the effect

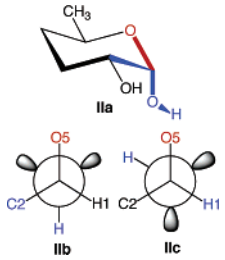

of an in-plane terminal electronegative substituent found in the α-Man configuration and that of an in-plane carbon substituent in the *β*-Man and *β*-Glc configurations (Figure S2, Supporting Information). No terminal effects are possible in the α-Glc configuration, but the internal substituent effect remains. Karplus curves derived for the four configurations (Figure 4B) were fit to give three unique eqs 14−16, since the curves for *β*-Glc and *β*-Man are virtually identical (separate equations for *β*-Glc and *β*-Man are given in Figure S2).

$$^3J_{C2,O1H}(\alpha\text{-Glc}) = 2.85 - 1.67\cos\theta + 3.20\cos(2\theta) - 0.25\sin\theta + 1.22\sin(2\theta) \quad R^2 = 0.99 \tag{14}$$

$$^3J_{C2,O1H}(\alpha\text{-Man}) = 3.60 - 3.35\cos\theta + 4.51\cos(2\theta) - 0.029\sin\theta + 0.85\sin(2\theta) \quad R^2 = 0.98 \tag{15}$$

$$^3J_{C2,O1H}(\beta\text{-Glc}/\beta\text{-Man}) = 3.33 - 1.56\cos\theta + 3.94\cos(2\theta) - 1.11\sin(2\theta) \quad R^2 = 0.98 \tag{16}$$

G. Couplings Involving OH6. Since the studies of $^3J_{HCOH}$ and $^3J_{CCOH}$ discussed above involve only secondary hydroxyl protons, *J*-couplings involving O6H were investigated to determine whether their behaviors are modeled satisfactorily by eqs 4, 10, and 11.

$^3J_{H6R,O6H}$ and $^3J_{H6S,O6H}$ were calculated in **13** using *Gaussian*03. The C2−C1−O1−CH_3, C1−C2−O2−H, C2−C3−O3−H torsion angles were set initially at 180° (little deviation

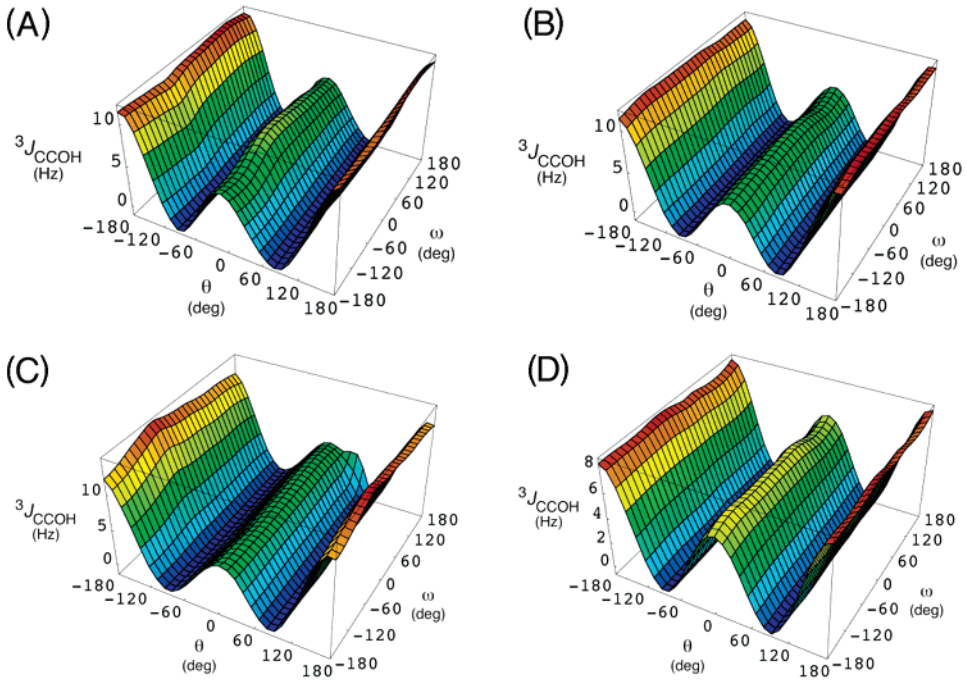

FIGURE 5. Dependence of $^3J_{C1,O2H}$ on ω and θ determined by DFT for **1** (A), **2** (B), **3** (C), and **4** (D). Note the strong dependence on θ and minimal dependence on ω. The maximal coupling observed in **4** (~8 Hz) is considerably smaller than observed in **1**−**3** (~11 Hz).

SCHEME 2

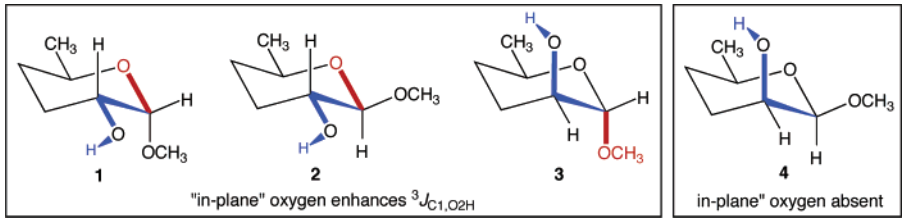

occurred during optimization from this initial value in each case), and the O5−C5−C6−O6 and C5−C6−O6−H torsion angles were fixed at 60°, −60°, and 180°, yielding nine structures. All other molecular parameters were optimized. The calculated couplings (data not shown) were superimposable on the curve in Figure 3, indicating that eq 4 is applicable and further supporting the use of a generalized equation to treat non-anomeric $^3J_{HCOH}$.

$^3J_{C5,O6H}$ values in **13** were influenced by the C5−C6−O6−H and the O5−C5−C6−O6 torsion angles (Figure 9). $^3J_{C5,O6H}$ is influenced by the orientation of O5. In-plane orientations (e.g., O5−C5−C6−O6 torsions near 180°; *tg* rotamers) enhance *anti* couplings by 3−4 Hz, whereas the effect is small for *gauche* couplings. The computed couplings were consistent with eq 10 for the *gg* and *gt* rotamers and eq 11 for the *tg* rotamer.

H. Studies of $^3J_{CCOH}$ in Simpler Model Systems. The effect of terminal substituents on $^3J_{CCOH}$ values was studied in two simpler model systems, ethylene glycol and *n*-propanol. In the former, the C−C−O−H torsion angle was fixed at 180° and the O−C−C−O torsion angle was varied in 30° increments through 360°. The calculated $^3J_{CCOH}$ was enhanced significantly by 4−5 Hz at an O−C−C−O torsion angle of 180° ($J \approx 14$ Hz) compared to couplings at 60° and −60° ($J \approx 9$−10 Hz) (Figure 10). This result is consistent with that observed in the more complex saccharide mimics. Calculations were conducted on *n*-propanol by systematically varying the C−C−C−O torsion angle in 30° increments while keeping the C−C−O−H torsion angle fixed at 180°. An enhanced coupling at a C−C−C−O torsion angle of 180° was observed (Figure 10), although the effect is smaller (~2 Hz) than that found in the diol. These results demonstrate that in-plane terminal substituents enhance $^3J_{CCOH}$ values, but the degree of enhancement depends on substituent electronegativity, with greater electronegativity yielding larger effects. It is therefore important to appreciate that the C1−C2−O2−H coupling pathway in β-Man (in-plane terminal oxygen absent) is not strictly comparable to the C3−C2−O2−H coupling pathway in α-Glc (in-plane terminal oxygen also absent) because the latter contains an in-plane terminal carbon (C4).

I. Solvation Effects on $^3J_{HCOH}$ and $^3J_{CCOH}$. The effect of solvent on the magnitudes of calculated *J*-couplings in **13** was investigated using *Gaussian*03 (see Computational Methods), and the results are found in Table S1 (Supporting Information). The difference in couplings calculated *in vacuo* and in solution is relatively small for couplings involving the hydroxyl protons and for solvent nonexchangeable nuclei. For $^3J_{HCOH}$ and $^3J_{CCOH}$, absolute differences of <0.5 Hz were observed. Absolute differences were larger for ^1J values (0−7 Hz for $^1J_{CH}$; 0.1−0.9 Hz for $^1J_{CC}$). Small absolute differences (<0.5 Hz) were observed for $^2J_{CH}$, $^2J_{CC}$, $^3J_{CH}$, and $^3J_{CC}$ except for $^2J_{C2,H1}$, which showed a change of 0.8 Hz.

J. C−O−H Coupling Pathways. $^3J_{HCOH}$ and $^3J_{CCOH}$ values exhibit strong dependencies on the central C−O torsion angle, with dynamic ranges of 8−15 Hz. In contrast, $^2J_{COH}$ values are

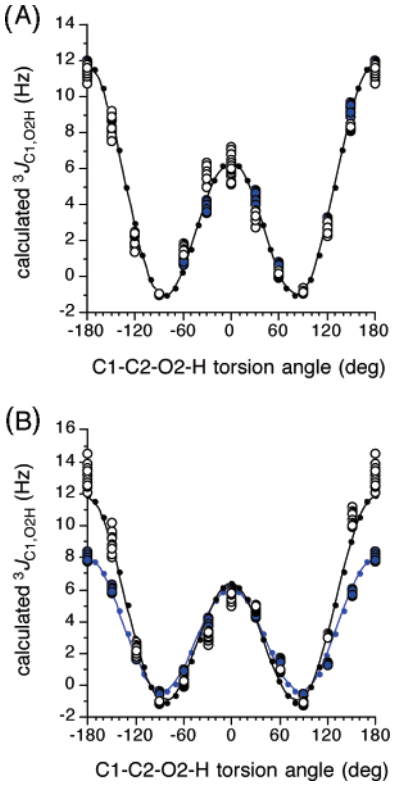

FIGURE 6. (A) Dependence of $^3J_{C1,O2H}$ on the C1−C2−O2−H torsion angle θ in **1** (open black circles) and **2** (closed blue circles) superimposed on the curve defined by eq 11. (B) Dependence of $^3J_{C1,O2H}$ on θ in **3** (open black circles) and **4** (closed blue circles), superimposed on the curves defined by eqs 11 and 10, respectively. The scatter at discrete torsion angles is due to the effect of ω.

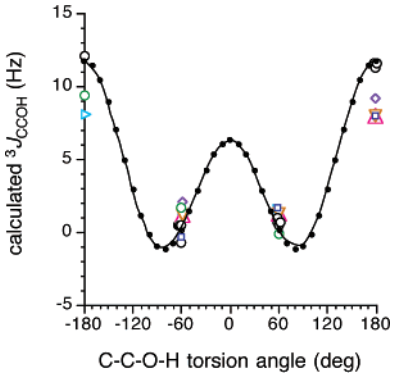

FIGURE 7. Dependence of $^3J_{C1,O2H}$ on the C1−C2−O2−H torsion angle based on eq 9 on which are superimposed $^3J_{C2,O1H}$ in **5**−**8**, $^3J_{C5,O4H}$ in **14**, $^3J_{C1,O2H}$ in **6** and **8**, and $^3J_{C1,O2H}$ in **9**−**12** for perfectly staggered C−C−O−H rotamers (60°, −60°, and 180°). Couplings are reduced at 180° for pathways lacking an in-plane terminal oxygen substituent on the coupled carbon (see text).

relatively small (−2 to −4 Hz), are negative, and display nonsystematic dependencies on C−C and C−O torsion angles (Figure S3, Supporting Information). These results suggest that $^2J_{COH}$ will not be a useful parameter to assess C−O conformation in solution.

II. Experimental Studies. A. Observation of OH Protons in 15−**20.** ^{1}H NMR spectra of **15**−**20** in H_2O/acetone-d_6 solvent at −20 °C contained sharp signals for the exchangeable hydroxyl protons (Figure 11). Resonance line-widths typically ranged from 2 to 3 Hz, and only moderate resolution enhancement was

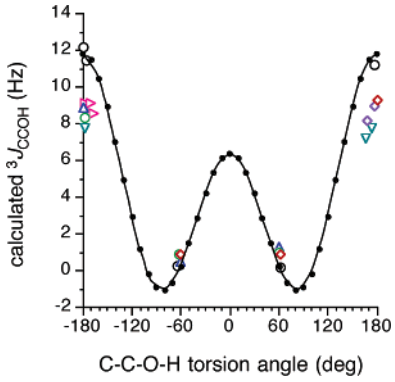

FIGURE 8. Dependence of $^3J_{C1,O2H}$ on the C1−C2−O2−H torsion angle based on eq 11 on which are superimposed $^3J_{C2,O3H}$ and $^3J_{C3,O2H}$ values in **9**−**12** computed for perfectly staggered C−C−O−H rotamers (60°, −60°, and 180°). Couplings are reduced at 180° for those pathways that lack an in-plane OH substituent on the coupled carbon (see text).

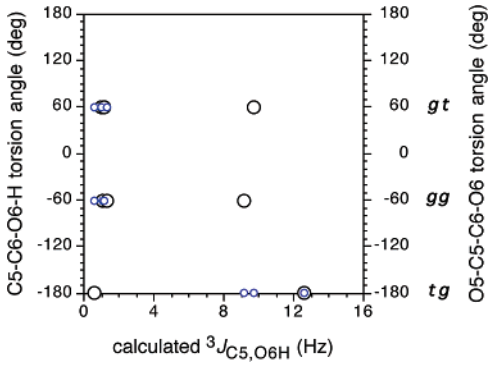

FIGURE 9. Effects of the C5−C6−O6−H (small blue open circles) and O5−C5−C6−O6 (large black open circles) torsion angles on $^3J_{C5,O6H}$ in **13**. The terminal in-plane O5 enhances the *anti* coupling in the *tg* conformation, whereas the effect on *gauche* couplings is negligible.

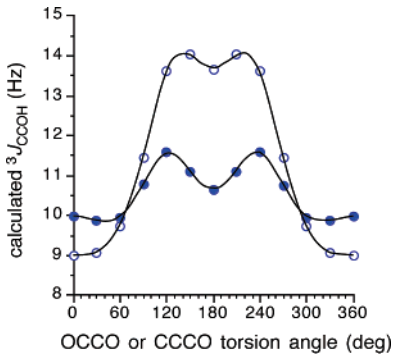

FIGURE 10. Calculated $^3J_{CCOH}$ in ethylene glycol (open circles) and *n*-propanol (closed circles) as a function of the O−C−C−O (glycol) or C−C−C−O (propanol) torsion angle. In both cases the C−C−O−H torsion angle was fixed at 180°.

applied to assist in *J*-coupling measurements. Nonexchangeable (CH) proton signals, which had typical line-widths of ∼1 Hz, were assigned on the basis of chemical shifts reported previously,[14,23] and exchangeable (OH) proton signals in **15** and **16** were assigned via selective ^{1}H-decoupling and/or 2D ^{1}H−^{1}H

(23) Hayes, M. L.; Serianni, A. S.; Barker, R. *Carbohydr. Res.* **1982**, *100*, 87−101.

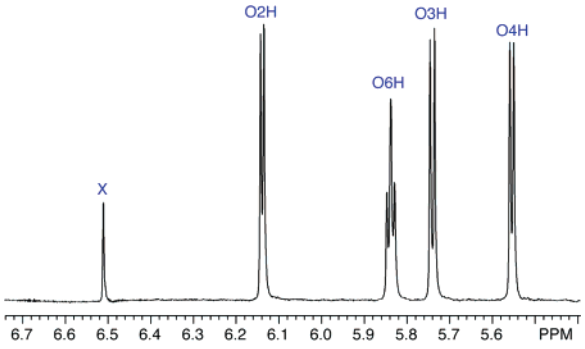

FIGURE 11. Partial 600 MHz ^{1}H NMR spectrum of **16** in 1:1 H_2O/acetone-d_6 at −20 °C showing signals due to the four exchangeable hydroxyl protons. The signal marked with an "X" is due to the OH protons of acetone *gem*-diol.

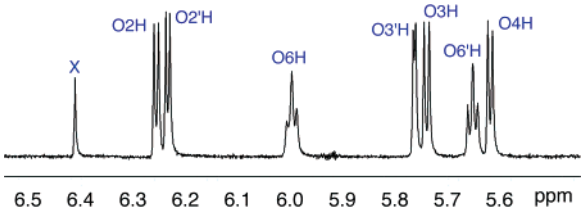

FIGURE 12. Partial 600 MHz ^{1}H NMR spectrum of **17** in 2:3 H_2O/acetone-d_6 at −20 °C showing signals due to the seven exchangeable hydroxyl protons. The signal marked with an "X" is assigned to the OH protons of acetone *gem*-diol.

COSY spectra. Hydroxyl proton signals in **17** were assigned using 2D ^{1}H−^{1}H TOCSY data (Figure S4, Supporting Information). Atoms in the Glc residue of **17**/**20** are denoted with primed symbolism, and those in the Gal residue are unprimed (see structure **17**).

The 1D ^{1}H NMR spectrum of **17** in 1:1 H_2O/acetone-d_6 at −20 °C contained overlapping resonances for O2H and O2′H, and for O3H and O3′H (data not shown). A change in solvent composition to 2:3 H_2O/acetone-d_6 eliminated these overlaps (Figure 12), yielding well-resolved doublets from which $^3J_{HCOH}$ could be measured reliably (Table 1). Similar analyses of **15** and **16** gave the *J*-couplings reported in Table 1. $^3J_{H4,O4H}$ and $^3J_{H6,O6H}$ in **16** are virtually identical to corresponding couplings observed in the Gal moiety of **17**. Larger differences were observed for $^3J_{H2,O2H}$ (∼0.6 Hz) and $^3J_{C1,O2H}$ (∼0.7 Hz) (Figures S5 and S6, Supporting Information), suggesting different preferred orientations of the C2−O2 bond in **16** and in the Gal moiety of **17**. $^3J_{H2,O2H}$ and $^3J_{H6,O6H}$ in **15** are virtually identical to corresponding values in the Glc moiety of **17**, but $^3J_{H3,O3H}$ decreases significantly from 5.1 Hz in **15** to 2.9 Hz in **17**.

With the exception of $^3J_{H3',O3'H}$ in **17**, $^3J_{HCOH}$ involving secondary alcohols range from 4.4 to 6.3 Hz. Since theoretical studies showed that Karplus curves for H−C−O−H coupling pathways are largely insensitive to pathway location (see above), the ∼2 Hz range in $^3J_{HCOH}$ for 2° OH groups suggests that C−O conformation differs from site to site in saccharides. $^3J_{H6,O6H}$ range from 5.5 to 5.7 Hz, and the pseudo-triplet character of the O6H/O6′H signals indicates rapid reorientation about C6−O6/C6′−O6′ bonds on the NMR time-scale. Application of eq 4 gave an averaged $^3J_{HCOH}$ of 5.7−5.8 Hz for (a) a freely rotating C−O bond, (b) free rotation involving three perfectly staggered rotamers that are equally populated, and (c) free rotation involving three staggered rotamers that are equally populated with deviations of up to 20° from idealized 60° torsion angles. These results are in good agreement with the experimental $^3J_{H6,O6H}$ and support the contention that some of the experimental $^3J_{HCOH}$, notably $^3J_{H2,O2H}$, do not reflect free rotation about their C−O bonds in solution. This conclusion is especially applicable to $^3J_{H3',O3'H}$ in **17**.

Similar calculations of $^3J_{CCOH}$ gave averaged values of ∼4.1 Hz (in-plane oxygen) and ∼3.4 Hz (no in-plane oxygen). These values are significantly larger than the experimental couplings, which range from 1.1 to 2.2 Hz, again suggesting that C−O torsional sampling is biased. Note that $^3J_{C4,O3H}$ decreases from 1.9 Hz in **15** to 1.1 Hz in **17**, a change that accompanies the large decrease in $^3J_{H3,O3H}$.[24e]

B. Inter-residue H-bonding in 17. X-ray crystal structures of **17**[24a] and related β-(1→4)-linked disaccharides[24b−d] show the presence of a single inter-residue hydrogen bond between O3′H and O5. The extent to which this H-bonding exists in aqueous solution remains an important question since this bonding could influence preferred linkage conformation and dynamics.

The glycosidic torsion angles ϕ and ψ assume values of 31.9° (H1−C1−O1−C4′) and −43.7° (C1−O1−C4′−H4′) in the crystal structure of **17**,[24a] and NMR studies[23] suggest values of ∼40° and ∼ −15°, respectively, in the predominant conformer in aqueous solution. Crystal structure analysis yielded crude H3′−C3′−O3′−H and C4′−C3′−O3′−H torsion angles of −43° and 78°, respectively, and $^3J_{H3',O3'H}$ and $^3J_{C4',O3'H}$ in **17**/**20** (Table 1) are consistent with *gauche* torsion angles in solution. The observed differences in both couplings in **15**/**18** and **17**/**20** may be caused by differences in the solvation of the Glc residue, resulting in different preferences of the C3−O3 bond torsion. Alternatively, formation of the glycosidic bond, which creates a new structural environment for H3′ and O5 at the linkage interface, orients them in close proximity and thus promotes the formation of a relatively persistent inter-residue H-bond. The much smaller $^3J_{H3',O3'H}$ observed in **17** relative to that in **15** illustrates that the preferred H3′−C3′−O3′−H torsion angle is context-dependent and that a stronger bias in favor of a *gauche* H3′−C3′−O3′−H torsion angle exists in the disaccharide.

If intra-residue H-bonding is responsible for the above-noted *J*-couplings in H_2O/acetone solution, then this bonding should be more persistent in nonprotic solvents like DMSO. The ^{1}H NMR spectrum of **17** in DMSO-d_6 (Figure S7, Supporting Information) contained well-resolved hydroxyl proton signals (see Figure S8 in Supporting Information for signal assignments and *J*-couplings). $^3J_{HCOH}$ measured in H_2O/acetone-d_6 (Table 1) and in DMSO-d_6 (Figure S8) were essentially unchanged except for$^3J_{H3',O3'H,}$ which is reduced to 1.3 Hz in DMSO. This finding is consistent with earlier work by Rivera-Sagredo et al.[24f] and suggests greater restriction of the H3′−C3′−O3′−H torsion angle in DMSO, possibly due to enhanced persistence of the putative H-bond.

J-Couplings observed in **15** and **17** were treated quantitatively using eqs 4 and 11, assuming a three-state model for the H3−

(24) (a) Stenutz, R.; Shang, M.; Serianni, A. S. *Acta Crystallogr.* **1999**, *C55*, 1719−1721. (b) Ham, J. T.; Williams, D. G. *Acta Crystallogr.* **1970**, *B26*, 1373−1383. (c) Fries, D. C.; Rao, S. T.; Sundaralingam, M. *Acta Crystallogr.* **1971**, *B27*, 994−1005. (d) Hirotsu, K.; Shimada, A. *Bull. Chem. Soc. Jpn.* **1974**, *47*, 1872−1879. (e) The accuracy of small *J*-couplings measured directly from hydroxyl proton signals will be affected by resonance line-width. When the line-width becomes comparable to the *J*-coupling, the observed splitting yields an apparent coupling that is smaller than the actual value by 0.2−0.3 Hz. Under these conditions, couplings should be determined by spectral simulation. (f) Rivera-Sagredo, A.; Jiménez-Barbero, J.; Martín-Lomas, M. *Carbohydr. Res.* **1991**, *221*, 37−47.

TABLE 1. Experimental $^3J_{HCOH}$ and $^3J_{CCOH}$ Coupling Constants[a] in H_2O/Acetone-d_6 Solutions[b] of 15−20

β-Glc **15/18**		β-Gal **16/19**		β-lactoside **17/20** (Glc ring)		β-lactoside **17/20** (Gal ring)	
coupled nuclei	coupling constant (*J*, Hz)	coupled nuclei	coupling constant (*J*, Hz)	coupled nuclei	coupling constant (*J*, Hz)	coupled nuclei	coupling constant (*J*, Hz)
H2−O2H	4.6	H2−O2H	4.5	H2′−O2′H	4.4	H2−O2H	5.1
H3−O3H	5.1	H3−O3H	6.3	H3′−O3′H	2.9	H3−O3H	5.9
H4−O4H	6.1	H4−O4H	5.5			H4−O4H	5.4
H6−O6H	5.6	H6−O6H	5.5	H6′−O6′H	5.6	H6−O6H	5.7
C4−O3H	1.9[c]	C1−O2H	2.2[c]	C4′−O3′H	1.1[d]	C1−O2H	1.5[d]
C4−O4H	−2.8[c]						

[a] In Hz ± 0.1 Hz. [b] At −20 °C; see Experimental Section for details. [c] ±0.2 Hz. [d] ±0.3 Hz

SCHEME 3. Definitions of Rotamers about the C3′-O3′ Bond in 17

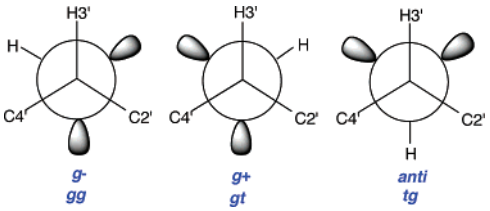

C3−O3−H bond torsion (Scheme 3). Using $^3J_{H3,O3H}$ and $^3J_{C4,O3H}$ of 5.1 and 1.9 Hz, respectively, rotamer populations were determined in **15** in H_2O/acetone-d_6: *gg*, ∼58%; *gt*, ∼14%; *tg*, ∼28%. The calculations thus predict unequal populations of the three rotamers in the monosaccharide. A similar treatment of the corresponding couplings for the Glc residue in **17** gave the following populations: *gg*, ∼85%; *gt*, ∼4%; *tg*, ∼11%. The significant increase in the *gg* population in **17** is consistent with the contention that inter-residue H-bonding between O3′H and O5 exists in this structure.

C. Hydroxyl Hydrogen Exchange Rates in 17 and Bridging Water. Hydroxyl hydrogen exchange rates for O3H and O3′H in **17** with solvent water showed no significant differences.[25] This result contrasts with studies of β-chitobiose **21** in

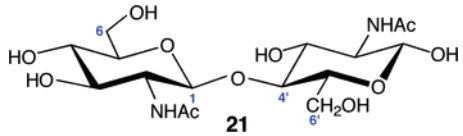

21

which a slower O3′H exchange rate was interpreted as support for an analogous H-bond between O5 and O3′H in solution.[26] Thus, if O3′H in **17** experiences an interaction with O5 in H_2O/acetone-d_6 solvent as suggested by the *J*-coupling data, the interaction does not reduce the solvent exchange rate as might be expected for a direct (i.e., no intervening water molecule is involved), relatively persistent H-bond. The lack of a solvent exchange effect might be explained if only a small percentage of molecules in solution experience a direct H-bond, or if the

SCHEME 4. DFT-Generated Bridging Water Complexed with 17; H_2O Molecule (blue box) Straddles the Glycosidic Linkage and Is in H-Bonding Contact with O5 and O3′H

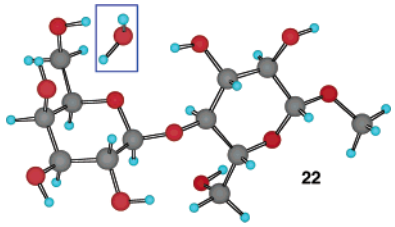

H-bonding is weak in all molecules. Alternatively, H-bonding mediated by a solvent water molecule (i.e., an indirect H-bond) could occur, which may not affect the exchange rate of the H-bonded hydroxyl proton. We examined whether a single water molecule could H-bond to **17** while satisfying the structural requirements dictated by the observed *J*-couplings. Using the crystal structure[24a] of **17** as a starting point, a water molecule was inserted arbitrarily near O3′H and O5 and the bimolecular complex geometrically optimized using DFT (B3LYP/6-31G*). Complex **22** emerged with the water molecule positioned above the plane of the Gal ring and in H-bonding contact with O5 and O3′H (Scheme 4). The H3′−C3′−O3′−H and C4′−C3′−O3′−H torsion angles in **22** are −54.9° and 65.4°, respectively, values similar to those observed in the crystal structure of **17**[24a] and consistent with the magnitudes of $^3J_{H3',O3'H}$ and $^3J_{C4',O3'H}$.

Conclusions

Hydroxyl proton orientation in solution is an important component of saccharide conformational studies. The high density of OH groups in these structures confers unique chemical and physical properties due to their ability to H-bond intra- and intermolecularly, notably in the latter case with solvent water. Prior work has shown that $^1J_{CC}$[13] and $^2J_{CCH}$[12] in saccharides provide useful information about exocyclic C−O rotamers in aqueous solution. This information, when used in conjunction with the $^3J_{HCOH}$ and $^3J_{CCOH}$ values studied here, should lead to firmer assignments of C−O rotamer populations in solution.

The present investigation shows that $^3J_{HCOH}$ depends primarily on the H−C−O−H torsion angle, is largely unaffected by adjacent C−O bond conformation, is largely unaffected by the type or location of the carbon bearing the OH group (except for those couplings sensitive to the C1−O1 torsion), and is modestly affected by non-Fermi contact contributions. These findings provide firm support for the use of a generalized Karplus equation to interpret non-anomeric $^3J_{HCOH}$ in saccharides. However, separate equations are needed to treat $^3J_{H1,O1H}$, because these couplings are subject to the additional effect of internal electronegative substituents. The latter effect causes

(25) Hydroxyl proton exchange rates were measured by saturation-transfer as described previously (Serianni, A. S.; Pierce, J.; Huang, S. G.; Barker, R. *J. Am. Chem. Soc.* **1982**, *104*, 4037−4044.). Hydroxyl proton signal intensities decayed exponentially as a function of water signal saturation time, and the decay time constant, τ_1, was related to the desired exchange rate constant, k_{ex}, by $1/\tau_1 = 1/T_1 + k_{ex}$, where T_1 is the spin-lattice relaxation time of the hydroxyl proton. T_1 was determined from the relationship, $M_z(\infty)/M_z(0) = \tau_1/T_1$. Rate constants of 1.1−1.7 s^{-1} (±0.3 s^{-1}) were observed at −20 °C in 2:3 H_2O/acetone-d_6. Measurements were made on a 600 MHz NMR.

(26) (a) Kindahl, L.; Sandström, C.; Norberg, T.; Kenne, L. *J. Carbohydr. Chem.* **2000**, *19*, 1291−1303. (b) Poppe, L.; van Halbeek, H. *Nat. Struct. Biol.* **1994**, *1*, 215−216.

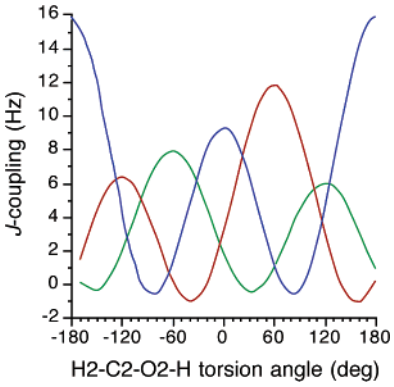

FIGURE 13. Plot of $^3J_{H2,O2H}$ (blue line), $^3J_{C1,O2H}$ (red line) and $^3J_{C3,O2H}$ (green line) for β-Glc **2** as a function of the H2−C2−O2−H torsion angle.

phase shifting of the Karplus curve partly due to the nonequivalent values of the *gauche* couplings. While the need for a separate set of equations to treat these couplings prevents use of a truly generalized $^3J_{HCOH}$ equation, it should be appreciated that analyses of H1−C1−O1−H torsions are only pertinent in reducing sugars; most analyses are likely to involve glycosides wherein only non-anomeric sites will be the focus of attention.

$^3J_{CCOH}$ is determined mainly by the C−C−O−H torsion angle as expected, but the orientation of terminal substituents on the coupled carbon, specifically oxygen and carbon, plays an important secondary role, with in-plane substituents enhancing the coupling when the coupled atoms are *anti*. The degree of enhancement depends on substituent electronegativity, with greater electronegativity yielding larger effects. For $^3J_{CCOH}$, generalized equations were obtained for coupling pathways containing an in-plane OH/OR or C substituent and for those lacking this arrangement. This effect is reminiscent of $^3J_{CCOC}$ behavior, which is affected by the orientation of terminal electronegative substituents on both coupled carbons.[11a] $^3J_{COCH}$ in saccharides may be influenced in a similar manner, although the effect is small and presently less well defined.[14]

Internal substituent effects influence $^3J_{C2,O1H}$ in a manner similar to $^3J_{H1,O1H}$, and thus separate equations are required to treat this coupling. The exact form of the equation depends on relative configuration at C1 and C2, since the mix of structural factors influencing this coupling varies with local structure.

The combined use of $^3J_{HCOH}$ and $^3J_{CCOH}$ is required to determine C−O rotamer populations in solution, and the parametrized Karplus equations developed here now make these treatments possible. For example, for the H2−C2−O2−H torsion angle in β-Glc **2**, $^3J_{H2,O2H}$, $^3J_{C1,O2H}$, and $^3J_{C3,O2H}$ exhibit the predicted dependencies shown in Figure 13. Experimental determinations of the three couplings provide redundant information to determine rotameric populations with greater confidence. This information can be combined with that obtained from $^1J_{CC}$[12] and $^2J_{CCH}$[11] to improve these analyses. The latter two couplings provide indirect C−O torsional information that, unlike $^3J_{HCOH}$ and $^3J_{CCOH}$, does not depend on the direct observation of the OH proton. In this sense, the two classes of couplings are complementary. Site-specific incorporation of ^{13}C at one or more sites in the saccharide facilitates not only the measurement of $^3J_{CCOH}$ values but also the assignment of OH signals and the measurement of these complementary $^1J_{CC}$ and $^2J_{CCH}$.

The magnitudes of some $^3J_{HCOH}$ and $^3J_{CCOH}$ observed in the mono- and disaccharides studied here are inconsistent with free rotational models about their constituent C−O bonds, suggesting that bias favoring specific C−O rotamers exists, at least under the solution conditions examined in this work. By comparing corresponding couplings in di- and oligosaccharides to related couplings in their constituent monomers, the effect of structural context can be evaluated, and thus information about solvent−solute interactions and/or the presence of inter-residue H-bonding may be obtained.

J-Coupling trends were found to be consistent with the presence of H-bonding between O3′H and O5 in the β-(1→4)-linked disaccharide **17** in H_2O/acetone solvent at low temperature. Prior studies of the β-(1→4)-linked chitobiose **21** by Kindahl et al.[26a] and of **17** in supercooled water[26b] have revealed anomalously small $^3J_{H3',O3'H}$ consistent with observations made in this study. These results were interpreted as suggesting the presence of weak H-bonding between O3′ and O5, albeit without confirmatory evidence provided by $^3J_{CCOH}$ and in the absence of Karplus equations derived specifically for saccharides. $^3J_{HCOH}$ values associated with highly preferred *anti* H−C−O−H torsion angles have also been reported as indicative of intramolecular H-bonding in sacccharides.[27] Interestingly, NMR studies of methyl α-lactoside **23** in this laboratory have revealed a $^3J_{H3',O3'H}$

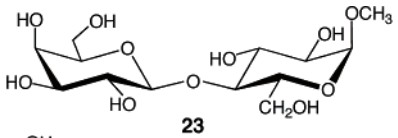

23

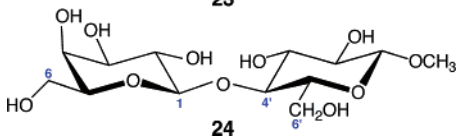

24

similar to that observed in **17** (Figure S9, Supporting Information), suggesting that the proposed inter-residue H-bonding may be a general characteristic of β-(1→4) linkages.

The strong bias in the H3′−C3′−O3′−H torsion angle in **17** in favor of a *gauche* conformation is a prerequisite for intra-residue H-bonding but does not prove its existence or indicate its strength. The preferred linkage conformation of **17** in aqueous solution, however, places O3′H in close proximity to O5 in a very high percentage of molecules, thus increasing the likelihood of this bonding. The strength of this interaction in aqueous solution remains uncertain, but recent studies[28] of $^1J_{CH}$ suggest an experimental means to answer to this question. $^1J_{C3',H3'}$ is expected to be influenced by C3′−O3′ bond conformation and by the strength of H-bonding involving O3′H.[29]

Future studies of the conformational implications of inter-residue H-bonding will benefit from access to glycosidic linkage

(27) (a) Sandström, C.; Baumann, H.; Kenne, L. *J. Chem. Soc., Perkin Trans. 2* **1998**, 809−815. (b) Sandström, C.; Baumann, H.; Kenne, L. *J. Chem. Soc., Perkin Trans. 2* **1998**, 2385−2393. (c) Sandström, C.; Magnusson, G.; Nilsson, U.; Kenne, L. *Carbohydr. Res.* **1999**, *322*, 46−56.

(28) Maiti, N. C.; Zhu, Y.; Carmichael, I.; Serianni, A. S.; Anderson, V. E. *J. Org. Chem.* **2006**, *71*, 2878−2880.

(29) A referee of this paper pointed out that the small $^3J_{H3',O3'H}$ observed in **17** reflects a marked change in the *time occupancy* of the H-bonded orientation. Hydroxyl group rotation still occurs under these conditions at a high rate (torsional frequencies of $\sim 10^9$ Hz), but presumably its time occupancy in the H-bonded state is enhanced. This fact may explain why no significant change in OH proton solvent exchange rate for the O3′H proton was observed. The same situation holds in DMSO-d_6 solvent; in this case, presumably stronger H-bonding further time biases the structure in favor of the *gauche* torsion, thus reducing the observed coupling to a smaller value than observed in H_2O/acetone-d_6.

interfaces containing different modes of inter-residue H-bonding. Modulation of the interface can be achieved, for example, by incorporating L-sugars into otherwise native di- or oligosaccharides. The inter-residue interface present in **17** is altered significantly when L-Gal is substituted for D-Gal, giving **24**. In the crystal structure of **24**,[30a] O2 and O3′ and O5 and O6′ are in close proximity, which is clearly different from the O3′H−O5 interaction observed in **17**. Preliminary measurements of $^3J_{HCOH}$ and $^3J_{CCOH}$ in **24** suggest H-bonding interactions between O6′H and O5 and between O2 and O3′.[30b]

Whether the detection of C−O torsional bias and/or inter-residue H-bonding in **17** are unique or will be observed more generally in di- and oligosaccharides remains an open and intriguing question. Glycosidic linkage conformation and dynamics in oligosaccharides are affected not only by well-known, albeit not fully understood, intrinsic stereoelectronic and steric factors, but potentially by nonbonded and other extrinsic factors. Inter-residue H-bonding comprises a subset of these extrinsic factors. Multiple water molecules interacting with saccharide solutes in aqueous solution may function as solvent-mediated H-bond bridges between adjacent or remote residues. This bridging, if reasonably persistent, could have significant implications for preferred linkage geometry, overall molecular topology, and dynamics. Indeed, bridging water molecules have been detected recently in molecular dynamics studies of disaccharides, and DFT calculations suggest that water can form specific bridging H-bonded complexes with disaccharides.[31−33]

Acknowledgment. This work was supported by grants from the National Institutes of Health (GM) (to A.S.). The Notre Dame Radiation Laboratory is supported by the Office of Basic Energy Sciences of the United States Department of Energy. This is document no. NDRL-4601 from the Notre Dame Radiation Laboratory. The authors also thank one of the referees for providing detailed discussion of hydroxyl group dynamics and the time bias of C−O rotations in solution.

Supporting Information Available: Table S1 showing *J*-couplings in **13** calculated *in vacuo* and aqueous solution using *Gaussian*03; Figure S1 showing the FC and non-FC contributions to calculated $^3J_{C1,O2H}$ in **2**; Figure S2 showing the dependence of $^3J_{C2,O1H}$ on the C2−C1−O1−H torsion angle in **6** and **8**; Figure S3 showing the dependence of $^2J_{C2,O2H}$ on θ and ω in **2**; Figure S4 showing the ^{1}H−^{1}H TOCSY spectrum of **17** in H_2O/acetone-d_6 (OH region); Figure S5 showing the ^{1}H NMR spectrum of **19** in H_2O/acetone-d_6 (OH region); Figure S6 showing the ^{1}H NMR spectrum of **20** in H_2O/acetone-d_6 (OH region); Figure S7 showing the ^{1}H NMR spectrum of **17** in DMSO-d_6 (OH region); Figure S8 showing the ^{1}H−^{1}H TOCSY spectrum of **17** in DMSO-d_6 (OH region); Figure S9 showing the ^{1}H NMR spectrum of methyl α-lactoside **23** in H_2O/acetone-d_6 (OH region) with $^3J_{HOCH}$ values; complete refs 17, 19, and 21; Cartesian coordinates for structures **1**−**14**, **22**, ethylene glycol, and *n*-propanol. This material is available free of charge via the Internet at http://pubs.acs.org.

JO0619884

(30) (a) Pan, Q.; Noll, B.; Serianni, A. S. *Acta. Crystallogr*. **2006**, *C62*, o82−o85. (b) Measurements of $^3J_{HCOH}$ and $^3J_{CCOH}$ in **24** labeled with ^{13}C at C1 in 2:3 H_2O/acetone-d_6 solvent at −20 °C gave the following values: $^3J_{H2,O2H}$, ∼3.0 Hz; $^3J_{C1,O2H}$, ∼3.0 Hz; $^3J_{H3,O3H}$, 6.0 Hz; $^3J_{H4,O4H}$, 5.5 Hz; $^3J_{H6,O6H}$, 5.1 Hz; $^3J_{H2′,O2′H}$, 4.6 Hz; $^3J_{H3′,O3′H}$, 4.4 Hz, $^3J_{H6′,O6′H}$, 6.3 Hz. These data reveal an increase in $^3J_{H6′,O6′H}$ to 6.3 Hz relative to that observed in **15** (5.6 Hz). Likewise, $^3J_{H2,O2H}$ and $^3J_{C1,O2H}$ differ in **16**/**19** and **24**, and $^3J_{H3′,O3′H}$ is reduced in **24** relative to the corresponding value in **15**. Taken collectively, these results support the presence of bias in the C3′−O3′, C6′−O6′, and C2−O2 bond torsions in **24**.

(31) Naidoo, K. J.; Chen, J. Y. *Mol. Phys.* **2003**, *101*, 2687−2694.

(32) Bosma, W. B.; Appell, M.; Willett, J. L.; Momany, F. A. *THEOCHEM* **2006**, *776*, 1−19.

(33) Bosma, W. B.; Appell, M.; Willett, J. L.; Momany, F. A. *THEOCHEM* **2006**, *776*, 21−31.